JOURNAL OF MATERIALS SCIENCE **36** (2001) 2133–2144

Off-axis creep of a ceramic-matrix/continuous-ceramic-fiber composite: Experimental evaluation

B. G. NAIR*, R. F. COOPER
Department of Materials Science and Engineering, University of Wisconsin-Madison, Madison, WI 53706 USA
E-mail: cooper@engr.wisc.edu

J. N. ALMQUIST, M. E. PLESHA
Department of Engineering Physics, University of Wisconsin—Madison, Madison, WI 53706 USA

The compression creep of a unidirectionally reinforced, SiC continuous fiber/calcium aluminosilicate (anorthite) glass-ceramic matrix composite was evaluated experimentally. Experiments covered the stress ($-\sigma_1$) and temperature (T) ranges of 20–40 MPa and 1300–1320°C, respectively. The experiments also emphasized characterization of the rheology as a function of the angle of misorientation (φ) between the applied compressive load and the direction of reinforcement. For any given σ, T condition, the highest steady-state strain rate occurred for $\varphi \sim 50^\circ$ (up to an order of magnitude faster than in the transverse, $\varphi = 90^\circ$, case); overall composite strain in this case included a substantial contribution from displacement across the fiber-matrix interface. The data reveal that the interfacial rheology responsible for the displacement is distinctly temperature sensitive. Evaluation of the composite flow through its comparison to numerical/rheological models that scrutinize the interfacial effect implies that the interface is characterized by a non-Newtonian viscous rheology; this suggests that the interface response involves specifically the flow of the thin amorphous silica interphase that comprises a portion of the fiber-matrix interface in this material. The overall plastic response of the unidirectionally reinforced material is nevertheless rate-limited by plastic flow of the matrix and can be described by the superposition of three modes of strain, the magnitude of each being dependent specifically on φ.

1. Introduction

Continuous fiber-reinforced ceramic-matrix composites (CMCs) are promising candidate materials for application as high-temperature structural materials. In addition to the intrinsic properties of monolithic ceramics (low density, good compressive strength, excellent heat resistance, corrosion resistance etc.), incorporation of the fibers is pursued to enhance other mechanical properties of the material such as its fracture toughness, wear resistance, fatigue strength and creep resistance. These unique and attractive combinations of material properties make CMCs excellent prospective materials for application as mechanical components in aerospace and automobile propulsion and power systems.

The ability to forecast the mechanical response of CMCs under typical operating conditions of low stresses, high temperatures and gradients of these conditions is of critical importance if CMC components are to be used successfully in the aircraft and/or automobile industry. The development of models to predict the behavior of a particular composite under these conditions is limited because of a dearth of relevant experimental data: a significant amount of work has been done on fracture of continuous fiber-reinforced composites and on developing composite design criteria based on fracture mechanics methodology; however, high-temperature creep has received distinctly less attention in the literature.

The bulk of experimental work done on creep of ceramic-matrix composites can be categorized into two types, based on specimen geometry: (i) tensile creep experiments with the maximum principal stress, σ_1, applied parallel to the direction of fiber reinforcement [1, 2] and (ii) flexural creep experiments with the reinforcing fibers parallel to the neutral axis [3–5]. For example, Holmes and co-workers [1, 2] studied the on-axis tensile creep and creep strain recovery behavior of fiber-reinforced glass-ceramic-matrix composites at

* *Present Address*: Ceramatec, Inc., Salt Lake City, UT 84119, USA.

high levels of applied stress ($[\sigma_1 - \sigma_3] \sim 60$–$250$ MPa; $T = 1200^\circ$C for CAS/SiC) and developed a numerical model incorporating bonded and debonded interface criteria to characterize the flow behavior. Not surprisingly, the tensile creep response of these composites was found to be governed by the creep behavior of the fibers as most of the stress is concentrated in the fibers due to extensive matrix microcracking and some matrix flow at high levels of applied stress. Alternatively, Weber *et al.* [3] demonstrated through flexural (fiber parallel to the beam axis) and compression creep experiments (fibers perpendicular to the applied stress) that the intrinsic anisotropy associated with unidirectionally reinforced composites can cause extensive dimensional distortions in transverse loading directions and concluded that the actual magnitude of this deformation depends on the explicit role of the "weak" interface. The specific role of such an interface on high-temperature creep of ceramic composites has not been addressed in detail in the literature.

Effort in creep studies in our group have been aimed at directly exploring the creep of continuous fiber-reinforced composites based on an understanding of the conditions required for creation of composites with (1) ambient-temperature toughness and (2) high-temperature thermochemical stability [6]. Enhancement of both of these properties is frequently accomplished through the use of a thin, "planar" (i.e. cylindrical-sheath) interphase separating fiber and matrix [7, 8]. It has been demonstrated through both numerical [9] and initial experimental studies [10] that the "worst case" scenario (i.e., conditions at which maximum creep rates are observed) is not the case of transverse loading. Maximum strain-rates are observed, rather, under conditions where the resolved shear-stress at the fiber-matrix interface is approximately maximized because of the orientation of fibers relative to the direction of the applied stress. The immediate goal of this investigation is to gain sufficient insight into the mechanisms contributing to the bulk high-temperature response of composite materials, so as to be in a position to know if the flow behavior of these materials can be described by a continuum model that accounts for all contributing physical mechanisms. The basic strategy is to address several important facets of the interface flow problem through carefully designed experiments that emphasize "off-axis" loading, and use the results to calibrate a coherent reliable analytical model that describes composite mechanical performance at elevated temperatures. The present work details and analyzes the experimental results of composite-creep.

2. Background to the off-axis deformation approach

Meyer *et al.* [9] developed a finite element model for high-temperature, off-axis compression creep of ceramic matrix composites. By "off-axis" we refer to a finite acute angle, φ measured between the loading direction and the reinforcing fibers (see inset in Fig. 1). The finite element model considered both bonded and debonded interfacial conditions; in the case of debonded interfaces, a Coulomb friction rheology, consistent with many ambient-temperature studies of fiber pullout during fracture, was employed to describe interfacial displacements during creep. The results of the model were compared to some high-temperature experimental composite rheology data on SiC fiber/aluminosilicate matrix composites obtained through creep and load-relaxation approaches [10]. The model predicts the development of a complex stress field around the fiber that evolves to a steady state; it additionally predicts the initiation of cavitation due to the development of tensile tractions at distinct locations (relative to the direction of the applied stress) of the fiber-matrix interface. The location (in directions perpendicular to that of the applied load) and extent of this type of predicted cavitation was verified in the initial experiments [10]. The bulk strain-rates of the composite are functions of the loading configuration characterized by φ, the matrix rheology, and very importantly, the mechanical response of the fiber-matrix interface. A composite with a debonded interface is found to be much more susceptible to large "off-axis" shear deformations due to matrix shear-flow combined with interfacial slip/displacement than a composite with a well-bonded interface. The experimental rheology data demonstrated behavior consistent with a debonded interface and could be modeled only by changing the friction coefficient (μ), describing flow at the interface from a value of 0.7 at 1300°C to 0.4 at 1310°C (i.e., the interface displacement dynamics appeared distinctly temperature sensitive). Contact friction, in general, does not have such characteristic temperature dependence. Therefore, the comparison of the model to these initial experiments really implies that some deformation mechanism other than Coulombic friction is operative at the fiber-matrix interface of the composite system studied. This work seeks to scrutinize specifically interface flow and its impact on bulk composite rheology.

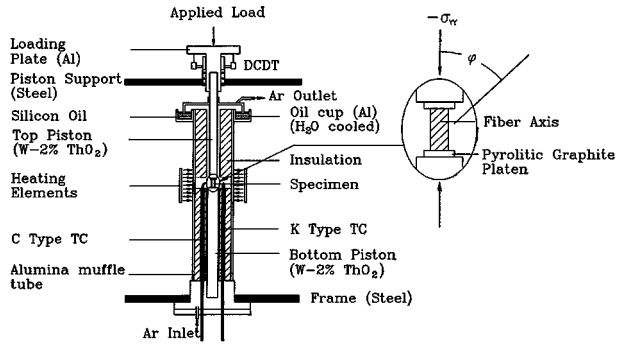

Figure 1 Experimental apparatus (furnace not shown for clarity) used for compression creep experiments (schematic). The inset illustrates the specimen geometry during the test. The misorientation angle φ is that between the fiber axis and the direction of the applied compressive stress, $\sigma_{YY} = \sigma_1$.

3. Experimental approach

3.1. Material specifications

The composite used for this study has a fine-grained matrix prepared by a glass-ceramic approach and SiC

TABLE I Composition of the calcium aluminosilicate matrix

Oxide	Specified[1] Wt. %	Actual[2] Wt. %	Actual[3] Mol. %
SiO_2	40.5	41.56	49.12
CaO	18.5	17.49	22.15
Al_2O_3	41.0	40.53	28.23
MgO	–	0.27	0.47

[1] Anorthite-corundum eutectic.
[2] X-ray fluorescence spectroscopy (XRAL Labs, Hamilton, Ont.).
[3] Calculated from weight-percent data.

continuous fiber (Nicalon ; Nippon Carbon Corp.) reinforcement. The composite is fabricated by the uniaxial hot-pressing of many prepreg plies to approximately 1350°C and 10 MPa and under an oxygen activity corresponding to the C:CO buffer [11]. The matrix, originally prepared as a mineral glass (melted in air at 1650°C for 16 hours), was batched corresponding to the anorthite ($CaAl_2Si_2O_8$)-corundum (Al_2O_3) pseudobinary eutectic (∼7 wt.% excess Al_2O_3). Elemental analysis was carried out on the matrix using X-ray fluorescence (XRF) spectroscopy (XRAL Laboratories, Hamilton, Ont.); the results are presented in Table I. Comparison of the actual composition of the matrix material to the batched composition seems to suggest that the matrix is depleted somewhat in CaO and enriched in SiO_2.

Electron microprobe analysis (CAMECA SX50) of the crystallized matrix indicated anorthite as the primary phase with small traces of mullite ($3Al_2O_3 \cdot 2SiO_2$) and silica (SiO_2). The matrix has a grain size of ∼3 μm with a distinctly equiaxed morphology. The fibers are ∼15 μm in diameter; the fiber volume fraction for composites used in this study is 0.3. There is ∼1% porosity in the as-pressed composites; the pores are widely spaced and vary in size from 1–3 μm. TEM observations of the fiber-matrix interface in the as-pressed composites show that it consists of two "planar" (i.e., cylindrical sheath) layers each of ∼80 nm thickness: the inner layer is graphitic carbon of grain size ∼1.5 nm; the outer layer is amorphous silica [12, 13]. These layers form as the product of an oxidation displacement reaction between fiber and matrix that occurs during composite fabrication. TEM also revealed that the fibers had crystallized during composite fabrication; dark-field imaging indicates a grain size for β-SiC of 1–1.5 nm [12, 13]. Specimens (3 × 3 mm in cross-section and 7.5 mm in height) were prepared with nominal values of 40, 50, 60 and 90 degrees for the misorientation angle (φ). The exact dimensions of each experimental specimen were measured precisely with a micrometer prior to creep deformation. Similarly sized creep specimens of unreinforced matrix were prepared, too, from a block of material that was fabricated following the same hot-pressing protocol used for composite fabrication. The grain size (∼3 μm) and grain morphology (equiaxed) of the unreinforced matrix specimens were the same as those of the matrix within the composite. The unreinforced matrix, however, had a slightly higher porosity (∼4%) than the matrix in the composite.

3.2. Apparatus

Creep experiments were conducted on a custom-made, dead-weight, controlled-environment creep apparatus, schematically shown in Fig. 1. The apparatus incorporated an electrical resistance furnace with $MoSi_2$ elements (model DT 31; Deltech, Inc., Denver, CO). Since these composites are unstable in an oxidizing atmosphere [13] as are the W-2% ThO_2 pistons, the tests were carried out in a high-purity argon atmosphere ($p_{O_2} \sim 10^{-6}$). Argon flow is maintained at a steady, low rate (gage pressure ∼ +100 Pa; flow rate ∼30 $cm^3 \cdot min^{-1}$) through an alumina tube that encloses the top and bottom pistons as well as the specimen. The gas is collected above a trough of silicon oil that serves as an essentially frictionless dynamic environmental seal [14]. The oil seal and piston mounts, which include the ports for thermocouples, are water-cooled.

Modeling of composite rheology, both analytical and numerical, is best accomplished following the assumption that the specimens deform homogeneously during creep. To ensure such homogeneity in actual experiments, pyrolytic graphite platens (dimensions ∼ 10 × 10 × 1 mm; Pfizer Inc., New York, NY) were used to separate the specimen from the pistons. With the orientation of the graphite basal planes along the plane of the platen (i.e., [0001] of the graphite is parallel to σ_1), the platens facilitate translation of the specimen ends. This orientation of the graphite platens insures that they do not creep at the temperature range of our experiments [15], and thus do not constitute a source of error in strain-rate calculations. Both these facts were verified by inspection of the deformed composite specimens (no barreling is seen) and through precision measurements of the thickness of the platens before and after a number of experiments. Temperature during the test was monitored and controlled using a W-5%Rh/W-26%Rh (Type C) thermocouple. The tip of the controlling thermocouple was ∼3 mm radially away from the center of the specimen. In a number of experiments, the thermal uniformity within the hot zone was confirmed with a second thermocouple by translating it vertically along the length of the hot-zone. The difference between the temperatures measured by the control and secondary thermocouples never exceeded 2°C; within the height of the specimen, the temperature variation was within ±1°C indicating a uniform temperature profile. During the experiment, the temperature fluctuation in the hot-zone was always less than ±1°C. The precision of temperature measurement of the apparatus is 0.5°C.

3.3. Test methodology

With the specimen in place, the apparatus was held at the experimental temperature for 4–5 h prior to the application of stress. Earlier experiments demonstrated that such an annealing period reduced significantly the extent of transient creep. We believe this behavior is related to the completion of the structural/chemical reaction creating the two interphases separating fiber and matrix and the establishment of steady-state matrix microstructure (i.e., completion of a structural reaction

between the anorthite matrix and the interfacial silica layer [16]). Stress was applied to the specimen by adding the appropriate weight (taking into account the weight of the piston, loading plate and oil-seal component) to the plate attached to the top piston. The displacement of the loading plate was measured directly using two direct-current differential transformers (DCDTs), mounted as shown in Fig. 1. The voltage output of the transducers was summed in analog form, digitally converted and stored on a microcomputer, utilizing a data acquisition program that was set to collect one voltage/time data point per minute (a rate amply fast for the slow creep rates encountered). Addition of pre-calculated incremental loads (lead shot) during deformation approximated constant stress conditions. These stress adjustments (weight additions) were made at displacements corresponding to each 0.1% of specimen strain. Usually, a composite specimen was crept to about 0.5% strain at each level of applied stress, enough to establish an apparent steady-state, after which the stress was increased to a higher level in a "loading" test or to a lower level in an "unloading" test. For most of the specimens, five stress levels were investigated, $-\sigma_{YY}(=-\sigma_1$; cf. Fig. 1) $= 20$, 25, 30, 35 and 40 MPa. The output of a typical loading test is shown in Fig. 2. The displacement jump observed with each change of load included the elastic deformation of the pistons as well as the specimen. The displacement data was converted to strain, and the steady-state strain-rates were calculated for the linear portions of each experimental segment by linear regression. Total inelastic strain in most cases was limited to ~2.5%. To test for the dependence of steady-state strain-rate on accumulated inelastic strain, in a number of experiments, the level of stress was dropped back to the initial value of 20 MPa at the end of a test for a final test segment.

The experiments were carried out at three different temperatures, 1300, 1310 and 1320°C, to study the thermal sensitivity of the high-temperature rheology. The fairly narrow range of temperatures selected was predicated primarily on material behavior. Initial experiments indicated an extraordinarily high "apparent" activation energy for composite creep, which meant that relatively small changes in temperature make substantial (and easily characterized) changes in strain-rate. ΔT of 10°C, while small on an absolute scale, was nevertheless large enough for resolution given the limits of our temperature control. Equally to the point, these temperatures were chosen because the matrix was designed for performance at 1300°C and these experiments therefore provide valuable information on the behavior of these composites at their limits of applicability.

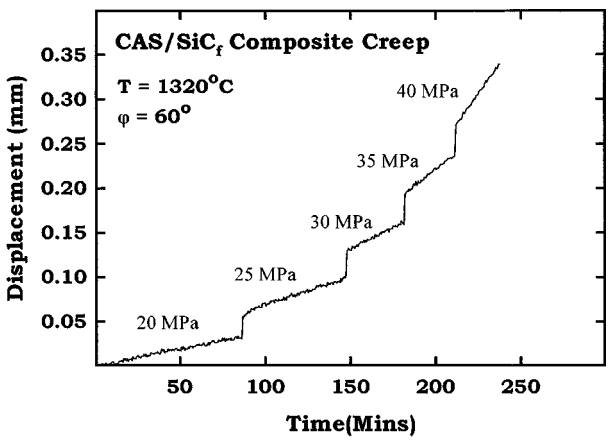

Figure 2 The output of a typical "loading" creep test. The spikes in displacement correspond to the elastic deformation of the column and specimen upon incrementing the load. Modest transients, on the order of $-\varepsilon_{YY} < 0.002$, are seen in the data (except at $-\sigma_{YY} = 40$ MPa). Noise in the data (±0.003 mm in displacement) is a result of thermal fluctuations.

The experimental assembly and approach for compression-creep experiments on the unreinforced matrix were the same as that used for the composites. In an effort to better understand the deformation mechanisms dictating the creep response of the composite, scanning electron microscopy and x-ray spectroscopy analyses were carried out on deformed composite specimens.

4. Results

4.1. Compression creep experiments: Composite

The experimental data were evaluated against the standard kinetic model for steady-state creep as a thermally activated phenomenon with a non-linear (power-law) stress dependence [17]:

$$\dot{\varepsilon}_{ss} = A\sigma^n \exp\left(-\frac{Q}{RT}\right), \tag{1}$$

where $\dot{\varepsilon}_{ss}$ is the steady-state strain rate, σ $(=\sigma_1 - \sigma_3)$ is the differential stress, n is the stress exponent, Q is the thermal activation energy, and RT has the usual meaning. In this loading geometry, $\sigma = \sigma_{YY}$ (cf. Fig. 1: $\sigma_1 = \sigma_{YY}$, $\sigma_2 = 0$, $\sigma_3 = 0$). A synopsis of the results of off-axis compression creep experiments is presented in Figs 3–5. The data indicate clearly (Fig. 3a and b) that the absolute steady-state strain rate of the bulk composite is distinctly sensitive to the orientation of the applied stress to the direction of reinforcement: one sees that the maximum strain rate is achieved in these experiments for the specimens with $\varphi = 50°$. Further, it is seen that composite flow is distinctly non-Newtonian: at 1320°C, an average n varies from approximately 3.7 at $\varphi = 90°$ to ~2.8 at lower angles (Fig. 3b). For any value of φ, the stress exponent is also dependent on the temperature: for $\varphi = 40°$ specimens, the average n increases from approximately 1.9 at 1300°C to about 2.7 at 1320°C (Fig. 4b). Despite the regression lines we have shown, the log $(\dot{\varepsilon}_{ss})$ vs. log (σ) data consistently show an upward curvature with increasing stress: n increases with σ. Solving for Q showed it, too, to be a very strong function of both φ and σ. In the standard Arrhenius plot of Fig. 5a, one sees that for a constant applied stress of -35 MPa, average Q varies from about 2290 kJ mol^{-1} for $\varphi = 40°$ to about 1635 kJ mol^{-1} for $\varphi = 90°$; in addition one sees that Q is also distinctly stress sensitive, as shown in Fig. 5b. Due to these high "apparent" activation energies (Q_{app}), the most conservative error-bars for all data presented were calculated based

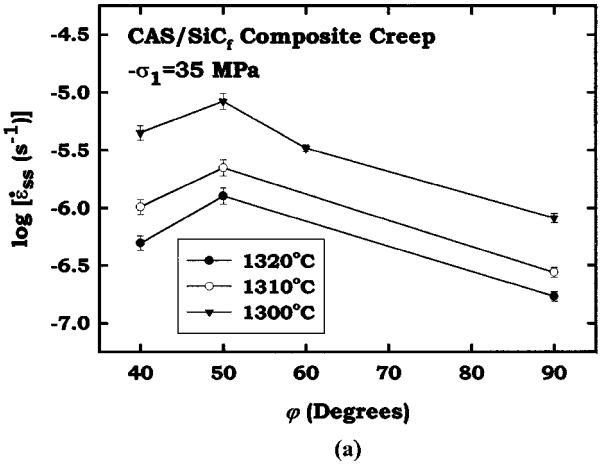

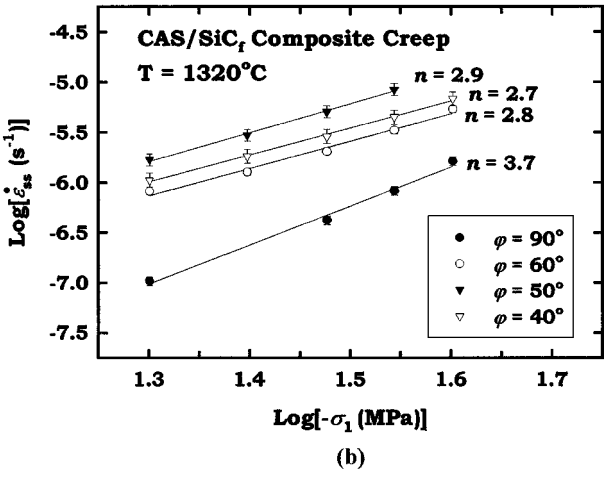

Figure 3 Composite steady-state creep response I. (a) Variation of steady-state strain-rate with φ for different temperatures at $\sigma_{YY} = -35$ MPa. Note that the maximum strain rate at all temperatures was observed for specimens with $\varphi = 50°$. (b) Variation of steady-state strain-rate with φ and $-\sigma_{YY}$ at 1320°C. Lines shown are linear regressions on each data set; values noted for the stress exponent, n, are slopes of the regression lines. Each data set demonstrates a consistent upward curvature, however: n increases with increasing stress for all φ (evident, too, in Fig. 4b).

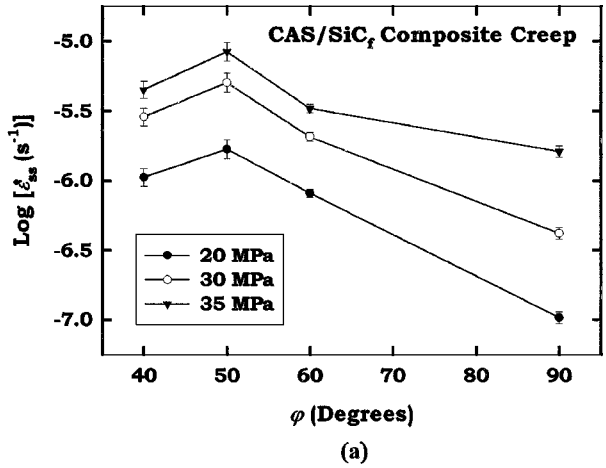

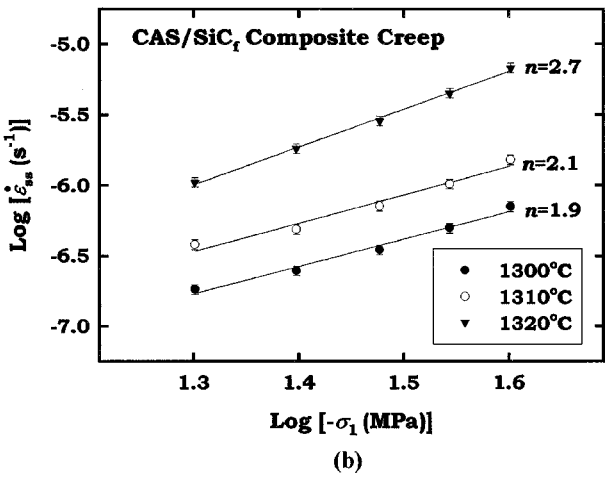

Figure 4 Composite steady-state creep response II. (a) Stress/strain-rate data for composite specimens with variation in φ. (b) Stress/strain-rate data for $\varphi = 40°$ specimens at different temperatures.

on our control of temperature during an experiment, i.e., the possible variation of strain-rates due to a change of ± 1°C in temperature for each value of φ was calculated as the error. The observed strain-rates in these cases were strikingly similar (within 20%) to the initial strain-rates, which indicated a strain-independence of the steady-state strain-rates at least at the low levels of total strain to which the specimens are subjected ($\sim$2.5%).

4.2. Compression creep experiments: Unreinforced matrix

The results of unreinforced matrix creep tests are shown in Fig. 6. In general, the matrix exhibited non-Newtonian behavior, with stress exponents that increased with applied stress. At 1300°C, n of the matrix material increased from about 1 (Newtonian behavior) at lower applied stresses ($\sim$20 MPa) to about 2 at higher stresses ($\sim$40 MPa). At 1320°C, the behavior of the matrix material was fully non-Newtonian, with $n \sim 1.5$ at the lower stress and increasing to $n \sim 2.5$ at higher stress levels. Even at 1320°C, however, the curvature of the data suggests that at stresses lower than the range studied (i.e., $<$20 MPa), the stress exponent might be close to Newtonian. As evident from this striking curvature in these data, the activation energy for creep, computed by fitting the data to Equation 1, was noted to be a function of the applied stress. Q for matrix creep increased from about 590 kJ mol^{-1} at $\sigma = 20$ MPa to about 810 kJ mol^{-1} at $\sigma = 40$ MPa.

Comparing these data to those for composite creep, one sees that the composite strain rates for the $\varphi = 50°$ specimens were slightly higher (1.5–2 times) than that observed for the polycrystalline matrix at similar stresses and temperatures, while those for the $\varphi = 40°$ and $\varphi = 60°$ specimens were comparable to those of matrix creep. The creep rates for the $\varphi = 90°$ specimens were about 7–10 times slower than those of the unreinforced matrix under similar (σ, T) conditions.

4.3. Microstructural investigation

Backscattered electron imaging of $\varphi = 90°$ specimens deformed to $\varepsilon_{YY} \sim 0.025$ (Fig. 7) showed cavitation of the fiber-matrix interface: cavitation occurred mostly within an angular width of 90° ($\theta = \pm 45°$–$135°$, where θ is the azimuthal angle measured along the fiber cross-section, cf. Fig. 8a) on either side of individual fibers.

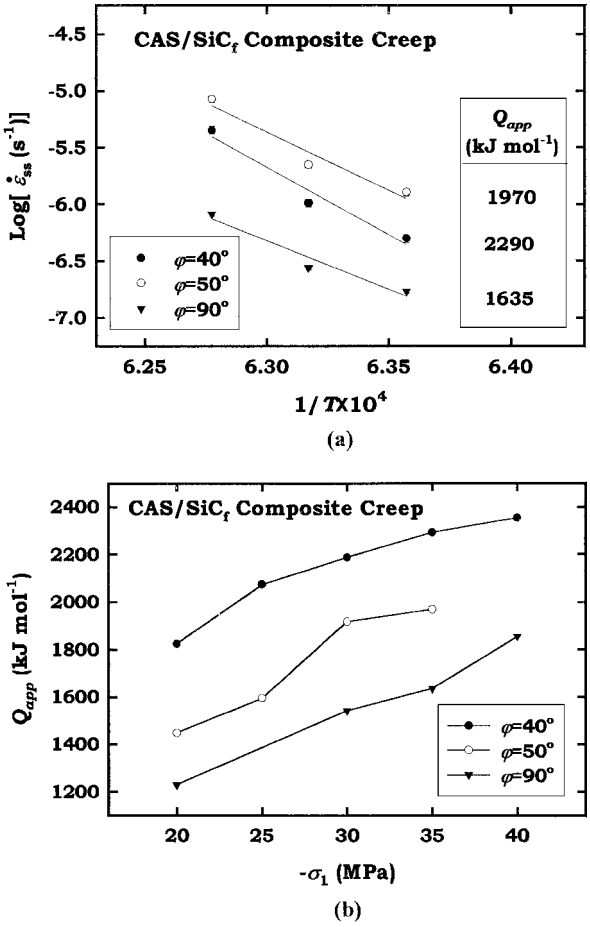

Figure 5 Composite steady-state creep response III. (a) Arrhenius plots for strain rate as a function of φ at $\sigma_{YY} = -35$ MPa. The apparent activation energies noted are based on the linear regressions shown. The data, however, demonstrate clearly an increase in Q_{app} with increasing T. (b) Variation of Q_{app} with σ and φ for composite specimens in the temperature range 1300–1320°C.

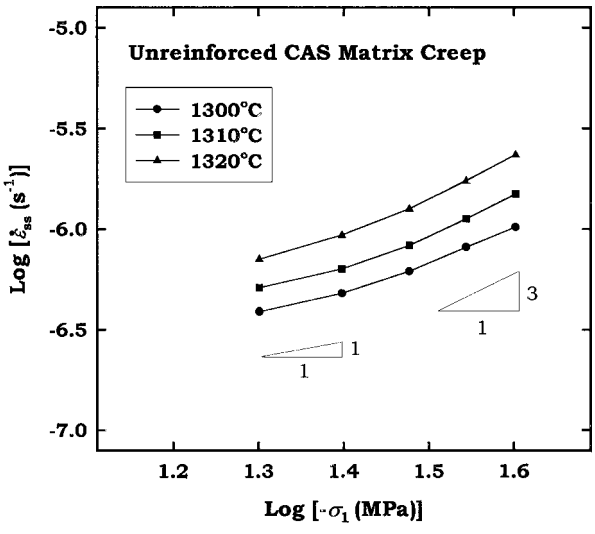

Figure 6 Creep response of the polycrystalline anorthite matrix as a monolithic ceramic. The variation of n from approximately 1 at low stresses to about 3 at higher stresses indicates a transition from a Newtonian (i.e., diffusional) rheology to a non-Newtonian (i.e., dislocation) rheology within this (σ, T) regime.

No other cavitation was noted in the matrix; however, by $\varepsilon_{YY} \sim 0.025$, one could find evidence of cavity linking nominally within the plane whose normal is perpendicular to σ (coalescence of these cavities provoked specimen failure at $\varepsilon_{YY} \sim 0.10$ [10]). Cavitation of the fiber-matrix interface was also observed in the $\varphi = 40^\circ$ specimens, though the extent was much less than in the transverse case.

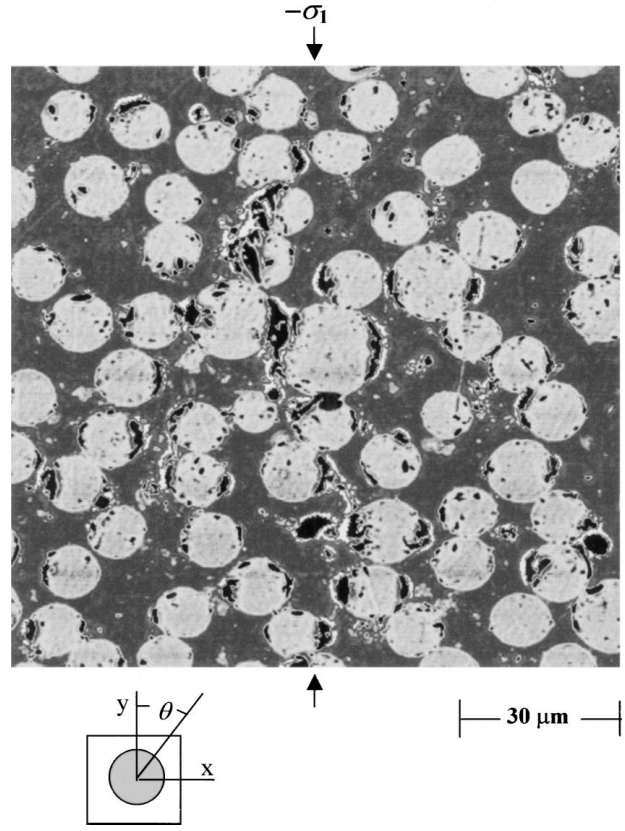

Figure 7 Backscattered electron image of a $\varphi = 90^\circ$ composite specimen, deformed to $-\varepsilon_{YY} \sim 0.025$, with the fibers in cross-section. The loading direction (in compression) is vertical. The microstructure is characterized by a significant amount of cavitation of the fiber-matrix interface perpendicular to the loading direction. The location of the interfacial cavitation is articulated by an azimuthal angle θ. The location and extent of this cavitation matches well the predictions of finite-element modeling [9] of composite rheology. There is evidence here of these interfacial cavities linking to initiate failure in the specimen; experience has shown that $-\varepsilon_{YY} \sim 0.010$ can be accumulated in specimens prior to their rupture.

5. Discussion

From the spectrum of creep data presented in Section 4, a number of general trends emerge as vital elements in our understanding of the plastic rheology of unidirectional composites:

(i) $\dot{\varepsilon}_{\text{ss}}$ for CAS/SiC$_{\text{f}}$ composites is a strong function of the misorientation angle, φ: the strain-rate is maximized at $\varphi = 50^\circ$.

(ii) n for composite creep is distinctly temperature sensitive in the stress-temperature regime scrutinized by our experiments: for off-axis composite specimens, n increases with T.

(iii) n for composite creep is higher than n for creep of the unreinforced matrix under similar conditions of σ_1 and T.

(iv) Q_{app} is a strong function of φ and σ_1: for a constant σ_1, Q_{app} increases with decreasing φ. For any specimen (fixed φ), Q_{app} increases with σ_1. The magnitude of Q_{app} was generally higher than that observed for the unreinforced matrix.

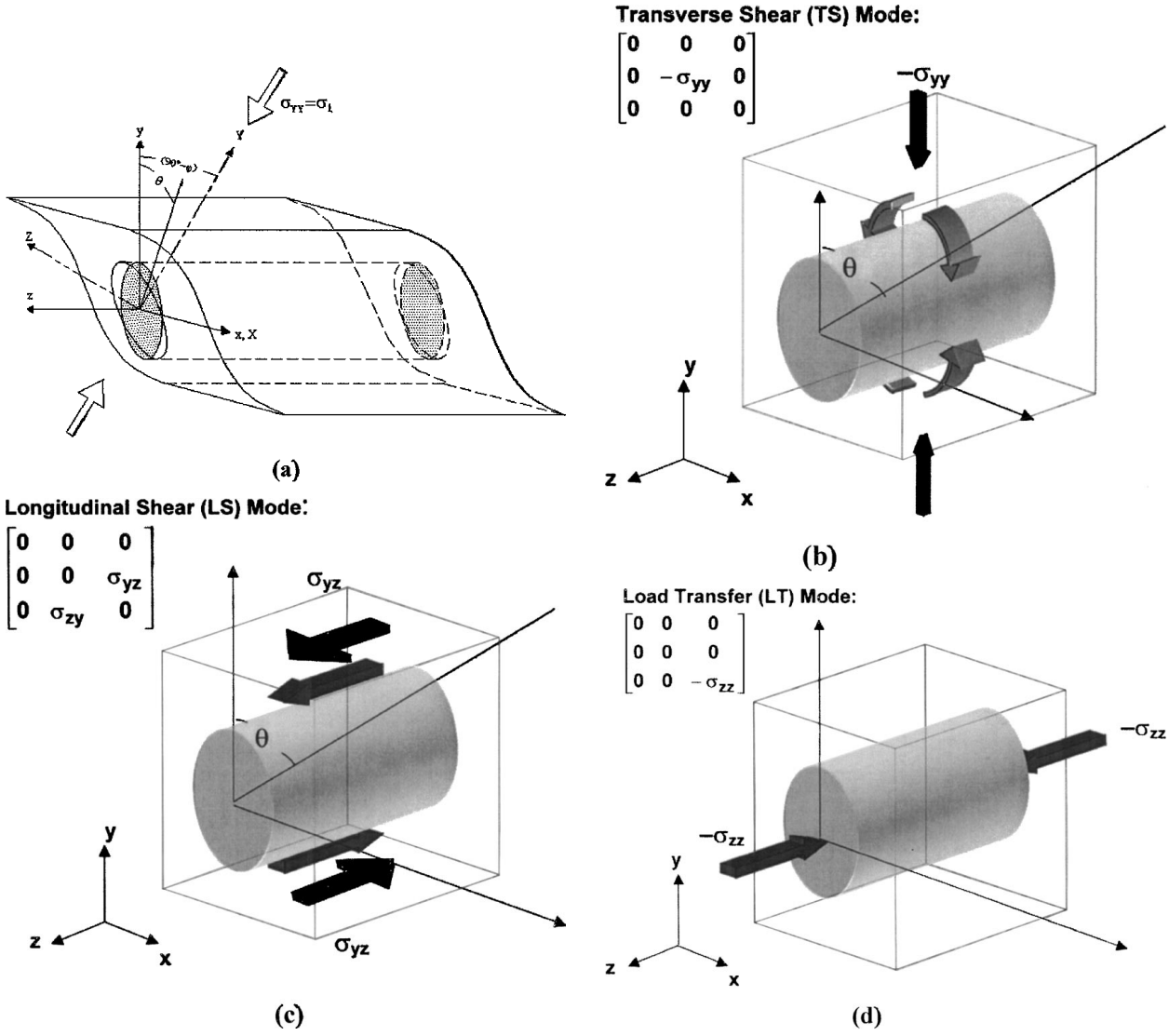

Figure 8 An approach to off-axis composite rheology. (a) Schematic representation of a deformed, originally tetragonal-prismatic unit cell of the composite in the compressional geometry that optimizes slip at the fiber-matrix interface (i.e., $\varphi = 50^\circ$). The coordinate system (X,Y,Z) describes the bulk composite specimen, while (x,y,z) describes the unit cell; $x \equiv X$ (cf. Ref [4]). $(90^\circ - \varphi)$ is the angle between y and Y. θ describes the azimuthal angle around the fiber moving clockwise from y to x. During composite creep, maintaining coherency of the matrix requires that any z-direction slip at the fiber-matrix interface must be accommodated by substantial flow in the matrix. (b) Transverse Shear (TS) mode characterized by matrix flow around the fibers due to resolved normal stress perpendicular to the fiber. (c) Longitudinal Shear (LS) mode characterized by shear flow of the matrix, slip at the fiber-matrix interface and rotation of fiber cross-section (primarily elastic in this case of a SiC/CAS composite) due to resolved shear stress in planes parallel to the fiber axis. (d) Load Transfer (LT) mode characterized by a long transient strain due to continuous transfer of stress from the matrix to the reinforcing fibers: steady-state would reflect creep of the fibers in this case.

(v) $\dot{\varepsilon}_{ss}$ is independent of the accumulated strain, ε, at least for $\varepsilon < 0.03$.

Any model that attempts to explain composite creep behavior should address and explain each of the effects noted above based on the rheologic behavior of the constituent phases (i.e., the matrix, fiber and the interface/interphase).

A survey of the literature for creep of Nicalon fibers suggests that under the range of σ_1 applied to the composite in our study (20–40 MPa), the creep-rates of the fibers are expected to be significantly lower than those observed for the unreinforced matrix. For the Nicalon fibers in these composites, the significant initial transient (and very high initial strain-rates) characteristic of non-crystallized fibers [18] is not expected as the fibers are completely crystallized during composite processing [13]. Crystallized (annealed) Nicalon fibers have a very high viscosity: two independent studies [19, 20] have shown that the fibers show Newtonian creep with $\dot{\varepsilon}_{ss} \sim 10^{-8}$ s^{-1} at $\sigma_1 \sim 300$ MPa. Extrapolation of this data to $\sigma_1 = 40$ MPa and the temperatures of our experiments indicates that the expected fiber strain-rates are at least two orders of magnitude lower than that of the matrix. Thus, in the analyses of these experiments and in contemplating low-stress, high-temperature creep of these composites, the fibers can be considered as elastic within the composites. An exception is the "on-axis" $(\varphi = 0^\circ)$ case, where load-transfer from the matrix to the fibers causes the actual stresses carried by the fibers at steady-state to be sufficiently high to produce an observable creep response [cf. 2].

The specific pattern of flow of the matrix within the composite is a strong function of the state of stress

developed in the matrix at steady-state: the steady-state stress distribution in turn is a function of φ. Fig. 8a shows a schematic of a deformed unit cell for a specimen with a misorientation angle, φ relative to $\sigma_{YY} = \sigma_1$. The (x,y,z) coordinate system, defined for the unit cell is related to the (X,Y,Z) system corresponding to the bulk specimen as shown in the figure: the x-axis for (x,y,z) system and the X-axis for the (X,Y,Z) system are identical and the angle between the z-axis and the Y-axis is φ. For unidirectional, fiber-reinforced composites, the components of the stress-tensor that are of significance in creep deformation are σ_{yy}, σ_{zz} and σ_{yz} $(= \sigma_{zy})$. Application of each of these components of the stress-tensor to the unit cell results in a specific pattern of behavior by the constituents of the unit-cell (i.e., the fiber, matrix and interface). In other words, three distinct "deformation modes" can be identified in such composites, namely the transverse shear (TS) mode (for σ_{yy}; Fig. 8b), the load-transfer (LT) mode (for σ_{zz}; Fig. 8d) and the longitudinal shear (LS) mode (for σ_{yz}; Fig. 8c). A mode of deformation can be defined as the viscoelastic response of the unit cell on application of an individual component of the stress tensor. Our approach to understanding composite rheology will be based on the idea that the actual creep response in generalized, arbitrary loading situations would be a superposition of the components of strains from the three deformation modes: the relative contribution of each mode to the bulk composite strain-rate is a function of φ, σ_1 and T. This approach is similar to that of the Levy-Mises equations [21] (flow rules) for continuum plasticity. Weighting factors for the contribution of the three modes are simple functions of the loading geometry, expressed through the variable φ, as well as of the relative moduli and effective viscosities of the composite constituents. While this approach involves some simplifying assumptions, it serves as an excellent analytical tool for understanding and quantifying the various deformation processes contributing to deformation.

Given that the fibers behave elastically, the composite creep response in off-axis geometries will reflect the behavior of both the CAS matrix and the fiber-matrix interface/interphase. Interface slip contributes to the overall strain-rate, but due to the fact that the matrix around the interface remains coherent/continuous during creep, such slip cannot occur without being accommodated by matrix shear flow (see Fig. 8a). Thus, slip at the interface and shear deformation of the matrix parallel to the fiber axes act as serial kinetic processes. It is important to note here that these geometrical constraints basically result in the requirement that interface slip (i.e. flow of the interphase) can never be rate-limiting even for the LS-mode where it contributes a substantial portion of the total strain. In other words, for all off-axis orientations considered in this study ($\varphi = 40$–90°), the overall response is rate limited by flow of the matrix.

The TS-mode is isolated by the transverse loading geometry ($\varphi = 90^\circ$). The presence of the high-stiffness Nicalon fibers causes the generation of a non-uniform stress-state in the matrix [9] in such a way as to maximize flow of the matrix around the fiber (cf. Fig. 8b). The steady-state von Mises stress (and $|\sigma_{yy}|$) in the matrix around the fiber is maximized at $\theta = 0^\circ$ and is the driving force for deformation. This increase in stress at $\varphi = 0^\circ$ has been confirmed through TEM studies of the matrix around the fiber that revealed a higher dislocation density at $\theta = 0^\circ$ as compared to $\theta = 90^\circ$ in a composite specimen subjected to high-temperature creep [22]. TS-mode deformation also leads to the development of tensile tractions at the fiber-matrix interface [9] at values of θ from $\pm 45^\circ$ to $\pm 135^\circ$. These tensile tractions cause debonding at the interface resulting in the predicable cavitation seen in Fig. 7. Some amount of recoverable elastic strain is also expected in this mode due to elastic compression of the fibers perpendicular to the fiber axes. Thus, mechanistically, TS-mode deformation is rate limited by matrix flow after a transient associated with the stress distribution around the fiber as shown with the spring-and-dashpot model in Fig. 9a. However, it should be noted that this simplified representation does not show the complex stress field developed in the matrix at steady-state that is crucial in understanding the specific response seen at $\varphi = 90^\circ$.

Subjecting a composite specimen to pure shear stress (i.e., σ_{yz}) parallel to the fiber axes can isolate the LS-mode. In addition to matrix shear, the resolved shear stresses in planes parallel to the fiber axis cause an elastic rotation of the fiber cross-section. The elastic distortion of the fiber is a result of the interface or

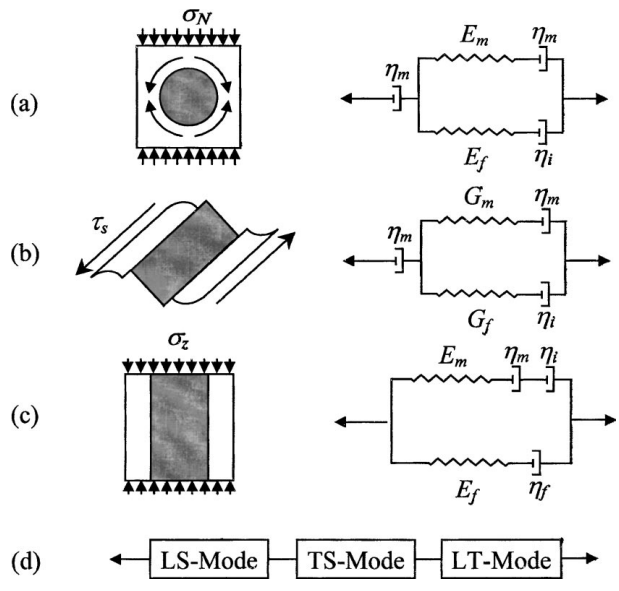

Figure 9 A kinematic model for the plastic rheology of unidirectional, continuous-fiber composites. ε_{YY} of a specimen is the accumulation of strain components from three distinct modes, based on the components of loading. In each case, simple spring-and-dashpot models are shown for each mode, although linearity of the viscous response in not implied. (Subscripts m, i, and f stand for matrix, interface and fiber, respectively.) (a) The Transverse Shear (TS) mode. (b) The Longitudinal Shear (LS) mode. (c) The Load Transfer (LT) mode, which is due to resolved normal stress parallel to the fiber axis, is ultimately rate-limited by the creep of the fibers. (d) In an analogy of the Levy-Mises flow rules, the overall strain of a composite specimen can be discerned from the simple superposition of the three modes of flow.

interphase(s) transferring load to the fiber. Thus, the transient response in the LS mode should be anelastic with a characteristic relaxation time dependent primarily on the viscosity of the interface. The mechanical model shown in Fig. 9b describes the LS-Mode: flow of the interphase and the matrix are serial kinetic processes. Thus the model illustrates that if $\eta_i \ll \eta_m$ (as is the case in the CAS/SiC_f composites), the creep behavior is simply rate-limited by matrix flow. In the extreme generalized cases of perfectly bonded and perfectly debonded interfaces also, rate-limitation is by matrix flow according to this model. This makes sense intuitively in relation to the unit cell as the matrix flow at $\theta = 0^\circ$ will be rate-limiting in a bonded case, whereas matrix shear flow at $\theta = 90^\circ$ will be rate-limiting for a perfectly debonded interface due to matrix continuity requirements. The geometrical constraint in this composite rheology case is usefully compared to the case of plastic flow in polycrystals, where there exists only a very small σ, T window where grain boundary sliding can actually rate-limit plastic flow [23].

In the LT-mode, the geometry imposes isostrain conditions on the fiber, matrix and interface. Subsequently, the stresses are partitioned between the fiber and matrix based on the volume fraction of each constituent. The length of the transient creep regime is determined the relaxation of the interface/interphase: if the interface can flow easily, the strain energy in the matrix is dissipated (i.e., the stress level is reduced) by interface slip. In effect, this means that the fiber is kinematically in series (mechanical "parallel") with the matrix and the interface as shown in Fig. 9c. If the viscosities of the matrix and the interface are much lower than that of the fiber (as in the case of these CAS/SiC_f composites), the model clearly shows that the steady-state creep response would be controlled by fiber flow provided the stresses in the fibers are high enough to initiate creep as seen in tensile creep experiments [2]. On unloading, the stored elastic energy in the fibers is dissipated by interface and matrix flow, resulting in a significant amount of strain recovery.

One method of verification of the superposition of modes approach is through study of the extent of predictable interfacial cavitation (cf. Fig. 7) as a function of φ. Such interfacial cavitation is a signature of the TS-mode of deformation. The fact that the extent of interfacial cavitation decreases systematically with φ (for similar levels of total strain) indicates that the contribution of TS-mode deformation to total strain decreases with decreasing φ. An important distinction must be made between cavitation initiated by debonding at the fiber-matrix interface and conventional intragranular and inter-granular cavitation initiated during creep of structural ceramics [24]. Matrix cavitation, frequently observed in high-T tensile creep of ceramics and ceramic composites, was neither expected nor observed in our compression experiments. The absence of such inter/intra-granular cavitation is because the hydrostatic (i.e., mean-normal) stresses developed in the matrix around the fibers at steady-state are compressive in most areas: the maximum tensile hydrostatic stress developed (assuming a debonded interface) was less than 5 MPa for $-\sigma_{YY} = 35$ MPa [9].

The superposition-of-modes approach helps to illustrate elegantly the features of the data noted at the beginning of this section. Of the three modes of deformation, the highest strain-rates are expected in the LS-mode: the reinforcing fibers contribute very little creep resistance in this mode and slip at the interface facilitates virtually unimpeded matrix shear deformation. The modeling pursued at Wisconsin [9, 25] scrutinizes specifically the LS-mode and shows that the strain-rates generated in the LS-mode are comparable to that of the unreinforced matrix. The slowest strain-rates are expected in the LT-mode, where steady-state behavior is rate-limited by creep of the fibers.

For the specimens with $\varphi = 40$–50°, the steady-state response is complex as all three modes of deformation occur simultaneously. However, the contribution due to the LS-mode is expected to be dominant as the "out-of-plane" shear stresses are maximized in these orientations. The notable difference between the composite strain rates at $\varphi = 50^\circ$ and $\varphi = 40^\circ$ may perhaps seem counter-intuitive, given that both these misorientation angles are equally removed by 5° from the planes of maximum shear stress within the specimen (i.e., the planes whose normal vectors are 45° removed from σ_1) and thus experience equivalent resolved shear stress (σ_{yz}). However, in the comparison of $\varphi = 50^\circ$ and $\varphi = 40^\circ$ creep responses, one realizes that, while both specimens experience very similar shear loading along the fiber-matrix interface, the $\varphi = 50^\circ$ specimen additionally retains a greater component of TS-mode loading and the $\varphi = 40^\circ$ specimen retains a greater component of the LT-mode. Since the strain-rates generated by the TS-mode are much higher than that for the LT-mode, it makes perfect sense that the $\varphi = 50^\circ$ show higher strain-rates.

The presence of the high-stiffness elastic fibers increases locally both the mean-normal stress and deviatoric stress within the matrix relative to the applied stress [9, 26]. The maximum mean normal compressive stress developed in the matrix at steady state (for $\sigma_1 = -35$ MPa, $\varphi = 90^\circ$) could be as high as 67 MPa for a debonded interface. At these higher stress levels, the expected deformation mechanism is dislocation creep of polycrystalline anorthite [27]. The trend of increasing stress-exponents and activation-energies shown by the unreinforced matrix in our experiments also demonstrates this transformation to dislocation creep at higher stresses. Indeed, composite specimens consistently displayed non-Newtonian creep behavior with stress-exponents ranging from 2 to 4 in this stress-temperature regime, suggesting that the matrix in the composite deforms by dislocation creep due to the high mean-normal stresses developed. A recent TEM study [22] by Sung and Hwang provides direct evidence of dislocation creep in CAS/SiC_f composites; high dislocation densities were observed at high-differential-stress regions in the CAS matrix (i.e. $\theta = 0^\circ$, as predicted by Meyer *et al.* [10]) following creep deformation. The actual stress distribution in the composite comprises of areas where the von Mises potentials are less than

that required for initiation of dislocation creep also. So, in reality, the n of the composite is an "average" stress-exponent indicative of the stress-distribution in the composite. This clearly explains the decrease in n with φ as the matrix deviatoric stresses are maximized at $\varphi = 90^\circ$ and their magnitude decreases with a decrease in φ. The temperature sensitivity of the composite stress exponent simply reflects the relative impact of temperature on the rheologies of the matrix and the interface. As T increases, the viscosity of the interface decreases, resulting in an increase in von Mises potentials in the matrix (cf. Fig. 8b and c), and correspondingly an increase in n.

The characteristic activation energy for dislocation creep [27] in polycrystalline anorthite is $Q_m \sim 1150\ \text{kJ mol}^{-1}$. However, the observed values for activation energy for the composite are much higher. To understand this behavior, it must be acknowledged that although the deformation occurs primarily through matrix flow, the observed activation energy of the composite is in fact an apparent activation energy, Q_{app}, which is quite different from the activation energy of the matrix. The composite strain-rate can be expressed as

$$\dot{\varepsilon}_{ss} = k\sigma_m^n \exp\left(\frac{-Q_m}{RT}\right) = k'\sigma_1^n \exp\left(\frac{-Q_{app}}{RT}\right), \tag{2}$$

where σ_m is the maximum von Mises stress in the composite matrix at steady-state and σ_1 is the far-field stress applied to the specimen. The stress exponent is the same in both sides of the equation as the composite reflects the n for dislocation-creep of the matrix. If $\sigma_{m(1)}$ and $\sigma_{m(2)}$ are the maximum von Mises potentials in the matrix at two different temperatures, T_1 and T_2 (with $T_1 > T_2$), respectively, Q_{app} can be expressed as

$$Q_{app} = Q_m + \frac{nR}{\left(\frac{1}{T_2} - \frac{1}{T_1}\right)} \ln\left(\frac{\sigma_{m(1)}}{\sigma_{m(2)}}\right). \tag{3}$$

A simple calculation, assuming $Q_m = 1150\ \text{kJ mol}^{-1}$ and $n = 3$, indicates that an increase in σ_m by 5 MPa (e.g., an increase of ~14% over a far-field applied stress of 35 MPa) created by an increase in temperature from 1300°C to 1320°C would translate into an apparent activation energy of $Q_{app} \sim 1560\ \text{kJ mol}^{-1}$. A difference of 10 MPa accompanying the same 20°C temperature increase produces $Q_{app} \sim 1935\ \text{kJ mol}^{-1}$. These values for activation energy are in excellent agreement with the actual values obtained for composite specimens in this temperature range. Thus, the higher Q_{app} at $\varphi = 40$–50°, in comparison to that at $\varphi = 90^\circ$, is simply due to the fact that the LS-mode is more conducive to slip at the interface. In other words, the same jump in temperature causes a comparatively larger increase in matrix von Mises potential for $\varphi = 40$–50°, resulting in a higher Q_{app}.

Our data, combined with the understanding of the structure of the fiber-matrix interface in the SiC/CAS composites, allows some reasoned speculation on the nature of the rheological response of the interface. The

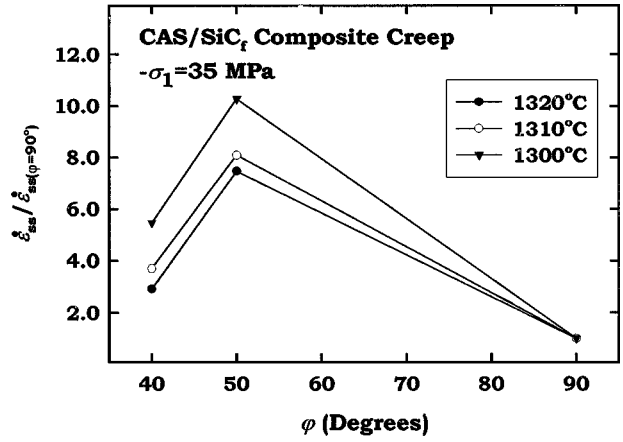

Figure 10 Composite steady-state strain rate ($-\sigma_{YY} = 35$ MPa) as a function of φ, normalized by the rate at $\varphi = 90^\circ$. That these different-temperatures curves do not overlap indicates that the displacements along the fiber-matrix interface accompanying deformation at $\varphi = 40^\circ$ and 50° involves a temperature-sensitive rheology for the interface.

data for the LS-mode (e.g., $\varphi = 50^\circ$) indicates clearly a temperature- sensitive, plastic flow response of the interface. Fig. 10 shows the data for creep of composite specimens normalized with respect to the strain-rates of $\varphi = 90^\circ$ at the same temperatures. The fact that the normalized curves do not coincide implies a thermally activated interphase rheology. An analytical model (outlined in Ref. 25) was developed specifically to study the rheological response of the LS-mode and to investigate various candidate interface models. The model employs a cylindrical unit cell, which is more amenable to analytical solutions and thus to the testing of various constitutive models for the interface than the tetragonal unit cell used in earlier finite element work. Interpretation of composite flow for $\varphi = 40$–50° employing the analytical LS-mode model suggests a temperature sensitive, non-Newtonian, viscoelastic (i.e., Maxwell) model is appropriate.

Structurally, one must conclude that this flow occurs in either or both of the two, planar reaction-layer interphases (nanocrystalline graphite or amorphous silica) that make up the interface in this material. Under compressive stress, graphite creeps only at exceedingly high temperature (>2000°C), with an activation energy of $Q \sim 1100\ \text{kJ mol}^{-1}$, and at such temperature the maximum strain rates reported [15] are $\sim 10^{-7}\ \text{s}^{-1}$. The displacement rate discerned here for the interface in the composite, when dissipated over an 80-nm-thick interphase, corresponds to a strain rate in the range 10^{-3}–$10^{-4}\ \text{s}^{-1}$. Extrapolation of the graphite creep data to temperatures and resolved stresses similar to those explored in the composite experiments indicates that its strain rate would be at least 10^4 to 10^5 smaller than that seen at the fiber-matrix interface. Thus, it is straightforward to conclude that flow of the carbon interphase is not important in the high-T rheological response of the composite interface.

In our CAS/SiC$_f$ composite system, there is evidence of substantial diffusion of Ca^{2+} and Al^{3+} ions into the interphase [12], which would suggest that the actual composition of the interphase is closer to a

multi-component silicate than it is to pure silica. Although fused silica deformed at strain rates $\leq 10^{-4}$ s^{-1} and under strictly anhydrous conditions displays a Newtonian viscosity with $Q \sim 750$ kJ mol^{-1} at equilibrium (i.e., when its structure has relaxed to that for the supercooled liquid at the temperature of interest) [28], more chemically complex silicate and aluminosilicate glasses are known to display a transition to non-Newtonian rheology as the strain rate (or stress) increases [29–31]. These observations, combined with our data and the analytical model [25], suggest clearly that it is non-Newtonian flow of the amorphous silica (silicate) interphase that dominates the interface rheology.

6. Summary/conclusions

High-temperature creep of continuous fiber-reinforced ceramic matrix composites is critically sensitive to the rheological properties of the fiber-matrix interface. This work has emphasized an experimental evaluation of the rheology of that interface in a unidirectionally reinforced SiC-fiber/calcium aluminosilicate (CAS; anorthite)-matrix composite. Our approach emphasized compressional-creep deformation experiments on bulk composite specimens where, along with exploring the stress and temperature sensitivities of flow, a primary variable of investigation was the angle (φ) between the reinforcement direction and that of the applied compressive stress. The experiments demonstrate clearly that the worst case for creep (i.e., the loading orientation producing the maximum steady-state strain rate for a given far-field applied stress) is not the transverse-shear case—fibers perpendicular to σ_1—but rather when the longitudinal-shear loading is maximized on the interface: for $\varphi = 50^\circ$, the steady-state strain rate of the composite was seen to be up to an order of magnitude faster than in the transverse case. The creep in this material under such loading includes a substantial amount of displacement on the interface; the experiments reveal clearly that this displacement constitutes a temperature-sensitive plastic flow of the interface. Comparison of the experimental data to an analytical model for flow at this φ indicates that the interface response is well characterized as a non-Newtonian Maxwell solid. The model interpretation, relative to our understanding of the structure of the SiC/CAS material, suggests that the interface rheology is actually flow of the thin, planar amorphous silica reaction-layer interphase that makes up a part of the interface. Despite the substantial contribution of interphase flow on the overall strain and strain rate of the composite at geometries favoring longitudinal shear (LS) loading of the interface, geometric compatibility insures that creep of the composite remains rate-limited by the flow of the matrix.

The ability to interrogate the rheology of the interface, albeit indirectly, through experiments that optimize the response of the LS mode and their comparison to an appropriate analytical model, is demonstrated here to be of particular importance in comprehending the plastic rheology of fiber-reinforced CMCs. The deformation-mode superposition approach should apply directly to the development of a continuum model for creep of composites, which is the ultimate goal of this and other, similar, composite rheology projects.

Acknowledgments

The composite material used in these experiments, while of our own design chemically, was fabricated at the Research and Development facility of Corning, Incorporated, Corning, NY, and was provided to us by Dr. Kenneth Chyung. We thank Dr. Chyung, too, for helpful discussions and his continued interest in our work. This research was financially supported, in part, by grant number DMR-9122687 from the Division of Materials Research of the National Science Foundation (U.S.A.).

References

1. Y. H. PARK and J. W. HOLMES, *J. Mater. Sci.* **27** (1992) 6341.
2. X. WU and J. W. HOLMES, *J. Amer. Ceram. Soc.* **76**(10) (1993) 2695.
3. C. H. WEBER, J. P. A. LÖFVANDER and A. G. EVANS, *ibid.* **77**(7) (1994) 1745.
4. F. ABBÈ, R. CARIN and J. L. CHERMANT, *J. Eur. Ceram. Soc.* **5** (1989) 201.
5. S. R. NUTT, P. LIPETZKY and P. F. BECHER, *Mater. Sci. Engr.* **A126** (1990) 165.
6. M. Y. HE and J. W. HUTCHINSON, *Int. J. Solids Structures* **25**(9) (1989) 1053.
7. J. B. DAVIS, J. P. A. LOFVANDER, A. G. EVANS, E. BISCHOFF and M. L. EMILIANI, *J. Amer. Ceram. Soc.* **76**(5) (1993) 1249.
8. P. E. D. MORGAN and D. B. MARSHALL, *ibid.* **78**(6) (1995) 1553.
9. D. W. MEYER, R. F. COOPER and M. E. PLESHA, *Int. J. Solids Structures* **29** (1992) 2563.
10. *Idem., Acta Metall. Mater.* **41**(11) (1993) 3157.
11. K. CHYUNG, R. F. COOPER, K. P. GADKAREE, R. L. STEWART and M. P. TAYLOR, U.S. Patent no. 4,615,987 (1986).
12. L. A. BONNEY and R. F. COOPER, *J. Amer. Ceram. Soc.* **73**(10) (1990) 2916.
13. R. F. COOPER and K. CHYUNG, *J. Mater. Sci.* **22** (1987) 3148.
14. B. L. MORDIKE, *J. Nucl. Mater.* **60** (1976) 223.
15. E. G. ZUKAS and W. V. GREEN, *Carbon* **6** (1968) 101.
16. R. F. COOPER, D. L. KOHLSTEDT and K. CHYUNG, *Acta. Metall.* **37** (1989) 1759.
17. H. J. FROST and M. F. ASHBY, "Deformation Mechanism Maps: The Plasticity and Creep of Metals and Ceramics" (Pergamon Press, Oxford, UK, 1982).
18. J. A. DICARLO and G. N. MORSCHER, in "Failure Mechanisms in High Temperature Composite Materials," ASME, AD 22, AMD 122 (ASME, 1996) p. 15.
19. G. SIMON and A. R. BUNSELL, *J. Mater. Sci.* **19** (1984) 3658.
20. R. BODET, J. LAMON, N. JIA and R. E. TRESSLER, *J. Amer. Ceram. Soc.* **79**(10) (1996) 2673.
21. G. E. DIETER, "Mechanical Metallurgy" (McGraw-Hill, New York, 1986) p. 89.
22. Y.-M. SUNG and S.-J. HWANG, *J. Mater. Sci.* **33** (1998) 5255.
23. E. W. HART, *Acta Metall.* **15** (1967) 1545.
24. S. M. WEIDERHORN, D. E. ROBERTS and T.-J. CHUANG, *J. Amer. Ceram. Soc.* **71**(7) (1988) 602.
25. B. G. NAIR and R. F. COOPER, J. N. ALMQUIST and M. E. PLESHA, *Mater. Res. Soc. Symp. Proc.* **365** (1995) 469.

26. T. L. DRAGONE and W. D. NIX, *Acta. Metall.* **37** (1990) 1759.
27. X. H. XIAO, A. DIMANOV, G. DRESEN and R. WIRTH, *EOS, Trans. Amer. Geophys. Union.* **77**(46, Suppl.) (1996) 716.
28. G. HEATHERINGTON, K. H. JACK and J. C. KENNEDY, *Phys. Chem. Glasses* **5** (1964) 130.
29. J. H. SIMMONS, R. K. MOHR and C. J. MONTROSE, *J. Appl. Phys.* **53** (1982) 4075.
30. S. L. WEBB and D. B. DINGWELL, *Phys. Chem. Minerals* **17** (1990) 125.
31. Y. BOTTINGA, *ibid.* **20** (1994) 454.

Received 20 September
and accepted 24 October 2000